Cement and Concrete Research 42 (2012) 321–326

Contents lists available at SciVerse ScienceDirect

Cement and Concrete Research

journal homepage: http://ees.elsevier.com/CEMCON/default.asp

Portlandite content and ionic transport properties of hydrated C_3S pastes

P. Henocq [a,*], E. Samson [a], J. Marchand [a,b]

[a] SIMCO Technologies Inc., 1400, boul. du Parc-Technologique, Quebec, Canada G1P 4R7
[b] Department of Civil Engineering, Laval University, Quebec, Canada G1K 7P4

ARTICLE INFO

Article history:
Received 24 January 2011
Accepted 6 October 2011

Keywords:
$Ca(OH)_2$ (D)
Ca_3SiO_5 (D)
Transport properties (C)
Diffusion (C)
Modeling (E)

ABSTRACT

This paper presents the results of a C_3S paste characterization study. The objective was to determine the parameters needed to model the process of degradation. The experimental study focused on determining the portlandite content and the ionic diffusion coefficients of C_3S paste. The molar C/S ratio of C–S–H in hydrated C_3S pastes was also investigated. The portlandite content was determined with an experimental method based on an electron microprobe analysis.
This method leads to a portlandite mass content of 24.4 ± 2.3%. The diffusion coefficient of each ionic species was determined by inverse analysis of diffusion test data performed on hydrated C_3S samples using a multi-ionic transport model.

1. Introduction

Tricalcium silicate (C_3S) is the major constituent of cement clinker. Its hydration produces two essential solid phases of the hydrated cement paste: calcium silicate hydrates (C–S–H) and portlandite (CH)[1]. In many cases, the behavior of cementitious materials in the presence of aggressive environments is controlled by the chemical properties of C–S–H and portlandite [1,2].

Hydrated C_3S pastes are only composed of C–S–H and portlandite when the hydration is complete [3]. These materials were often used during the past decades to characterize the hydration process of C_3S, the C–S–H and CH formation, and the chemical equilibrium of these hydrates in various conditions. The mechanisms of C_3S hydration were investigated to describe the different steps of the C–S–H formation and portlandite precipitation [4]. The molar C/S ratio of C–S–H in hydrated C_3S pastes varies between 1.2 and 2.1 [5–8]. This variation depends on the studied systems and also on the measurement techniques. Other studies were performed to characterize portlandite resulting from cement hydration. Experiments were conducted to determine the portlandite mass content in hydrated C_3S pastes. According to the literature, values vary from 25% [9, 10] up to 35% [11–13].

The present work focuses on the characterization of hydrated C_3S pastes. The objective is to gather information that can be used later to analyze leaching tests performed on the same material. Such a study requires having fundamental properties of the tested material such as porosity, solid phase contents, and ionic diffusion coefficients. Due to small sample sizes, their determination required specific and innovative experiments. The portlandite mass content of the hydrated C_3S pastes, and consequently the C–S–H mass content, were determined from an electron microprobe analysis. In addition, the well-known thermogravimetric measurement has been used. The diffusion coefficient is a significant parameter of the rate of chemical attack. However, no data is available on the ionic transport properties in the case of C_3S pastes. This paper presents the determination of the ionic diffusion coefficients from diffusion tests performed on hydrated C_3S pastes. The diffusion tests were analyzed by inverse analysis using STADIUM®, a reactive transport model specifically designed for cementitious materials [14].

2. Materials

C_3S paste samples were hydrated for 25 years in saturated lime water. The specimens were thin discs of 1.5-mm thickness and 22 mm in diameter made from compacted C_3S pastes [15]. The water-to-C_3S ratio was 0.5. Full hydration of the specimens was assumed and it was also assumed that they were only constituted of C–S–H and portlandite. The complete hydration was confirmed by SEM micrography with a JEOL 840-A apparatus (Fig. 1). Only two major solid phases were identified by SEM: C–S–H in grey and portlandite in white, as shown in Fig. 1(a). Unhydrated C_3S particles were not detected. Fig. 1(b) confirmed that the hydrated C_3S paste was a compact C–S–H and portlandite mix, without significant compaction voids. At the scale of the material, the C–S–H and portlandite phases were uniformly dispersed. The cracks, shown in Fig. 1(a) and (b), were caused by the surface preparation of the sample. The porosity has been estimated at 35% from the mass loss after freeze-drying a saturated sample. The total evaporation of all the water by freeze-drying was assumed. The saturation of a C_3S paste sample after drying under vacuum led also to a porosity equal to 35%. The result was in accordance with a previous work on similar C_3S

* Corresponding author.
E-mail address: phenocq@simcotechnologies.com (P. Henocq).

[1] In this paper, conventional cement chemistry notation is used, i.e. C = CaO, S = SiO_2, H = H_2O.

0008-8846/$ – see front matter © 2011 Elsevier Ltd. All rights reserved.
doi:10.1016/j.cemconres.2011.10.001

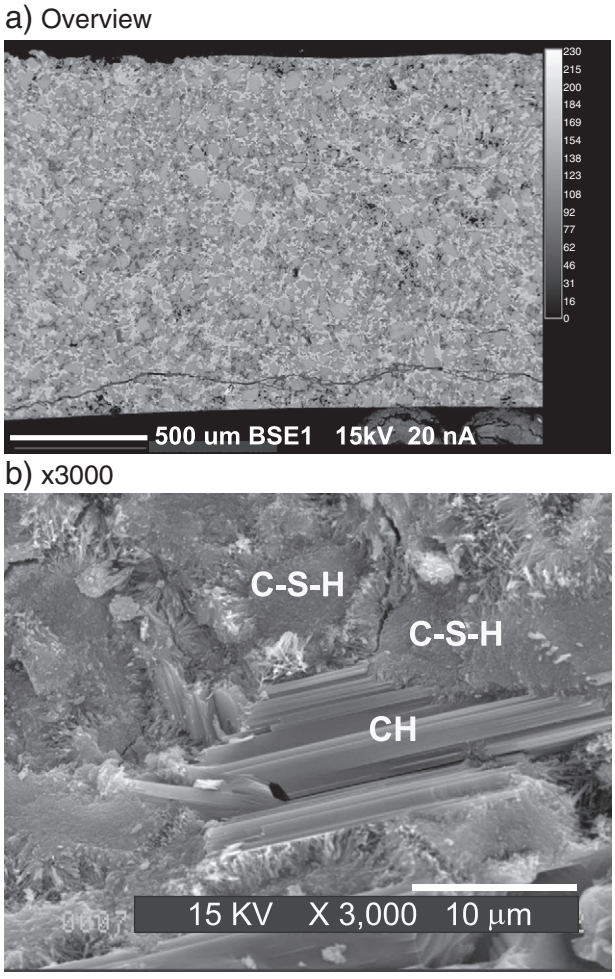

Fig. 1. SEM micrographs of polished slices of sound hydrated C_3S paste.

compacts [15]. Other studies on hydrated C_3S pastes gave a porosity between 35% and 45% [3] or between 30% and 40% [16] for similar water-to-binder ratio. Before porosity tests, the C_3S samples were immersed in alcohol (isopropanol) for one week and dried in a vacuum chamber for one week.

3. Microprobe experiments

3.1. Analysis

The calcium and silicon contents were measured by electron microprobe measurements (Fig. 2(a)). The experiments were performed with an electron microprobe CAMECA SX-100 along the thickness of the C_3S samples. The calcium and silicon contents were measured from K-alpha lines using LPET and TAP crystals respectively. The electron beam was defocused at 10 µm. The voltage was 15 kV and the beam current was 20 nA. Each profile contained 500 points for a thickness around 1200 µm; the resolution of the profiles was closed to 2.5 µm. Four hydrated C_3S specimens were analyzed by microprobe; a total of 10 profiles was made.

At the material scale, the homogeneous composition of the C_3S paste was confirmed by the calcium and silicon microprobe profiles; the peak amplitude of calcium and silicon profiles remained constant across the sample thickness. As seen in Fig. 2(b), the different solid phases in the hydrated C_3S could be identified. The presence of portlandite was associated to a calcium peak corresponding to a silicon content equal to zero. The SEM micrograph in Fig. 1(b) showed that the crystal size of the minerals was greater than 10 µm. The precision of the beam width

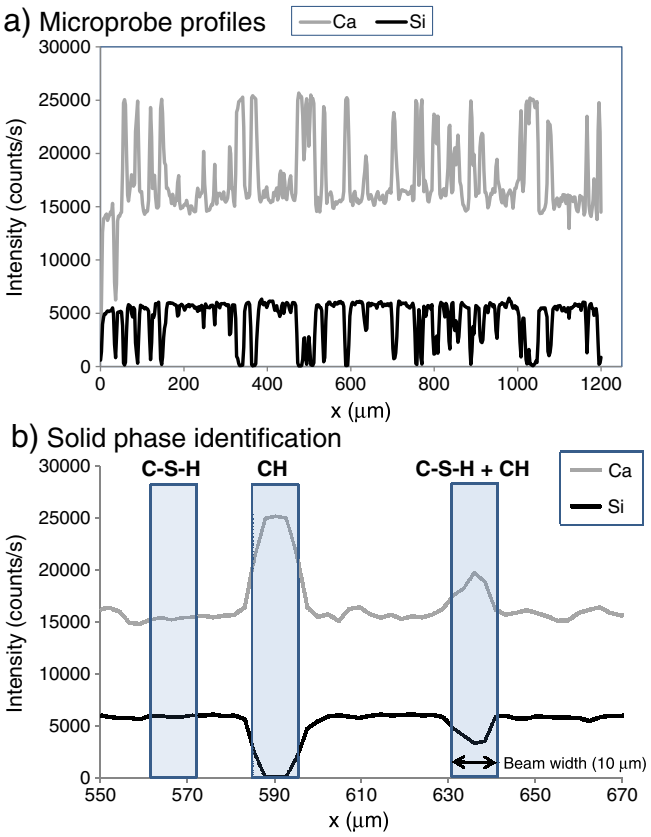

Fig. 2. Microprobe profiles on polished slices of sound hydrated C_3S paste.

(10 µm) and the distance between two measurements (2.5 µm) allowed to precisely locate the solid phases. As shown in Fig. 2(b), the presence of C–S–H in the profiles is associated with locations where calcium and silicon profiles are matching each other. In other locations, calcium peaks are associated with low values of silicon count, indicating the presence of portlandite crystals and C–S–H.

The calcium and silicon contents were measured in counts/s (Fig. 2). These contents are proportional to the mass concentration of each element and this relationship depends on the beam current [17]. The measured value can be converted in mass percentage for each element using mineral standards. In this work, the portlandite, which is a well-crystallized solid phase, was used as calibration standard to provide the conversion factor of the mass concentration of calcium. As previously mentioned, the portlandite was clearly identified from microprobe profiles (Fig. 2(b)). The number of counts associated to the portlandite was reproducibly measured for each profile at 25,200 counts/s while the calcium mass concentration in portlandite is 54%. Consequently, the conversion factor for calcium is estimated at 467 counts/s/% for a current beam of 20 nA. This value is in accordance with the value of 485 counts/s/% obtained on diopside from microprobe measurements performed with the electron microprobe CAMECA SX-100.

C–S–H was used to determine the mass conversion factor of silicon. C–S–H can be written as $xCaO–SiO_2–nH_2O$ where x is the molar C/S ratio and n is the molar H/S ratio. The mass concentration of calcium $Ca^{\%mass}_{C-S-H}$ and silicon $Si^{\%mass}_{C-S-H}$ in C–S–H are respectively given by:

$$Ca^{\%mass}_{C-S-H} = \frac{xM_{Ca}}{xM_{CaO} + M_{SiO_2} + nM_{H_2O}} \quad (1)$$

$$Si^{\%mass}_{C-S-H} = \frac{M_{Si}}{xM_{CaO} + M_{SiO_2} + nM_{H_2O}} \quad (2)$$

where M_{Ca} is the molar mass of calcium (40.08 g/mol), M_{CaO} is the molar mass of calcium oxide (56.08 g/mol), M_{Si} is the molar mass of silicon (28.09 g/mol), M_{SiO_2} is the molar mass of silicon oxide (60.08 g/mol), and M_{H_2O} is the molar mass of water (18.02 g/mol).

The molar H/S ratio is required to determine the mass concentration of calcium and silicon in C–S–H. The C_3S paste samples have been dried under vacuum for one week prior the microprobe analysis. The C–S–H were assumed to keep all their initial chemical water during the process. In these conditions, the molar ratio H/S is taken at 2.1 in accordance with the formulation of jennite $C_{1.67}SH_{2.1}$ given in Ref. [18]. The calcium content in box C–S–H was measured at 16,500 counts/s; it corresponds to a mass concentration of 35.3% with the conversion factor of 467 counts/s/%. By considering H/S equal to 2.1, the molar C/S ratio is estimated from Eq. (1) at 1.71, which is close to the C/S of the jennite as previously defined by Ref. [18]. Then, according to Eq. (2), the mass proportion of silicon in C–S–H is 14.5%. The silicon content in C–S–H has been measured at 6200 counts/s (Fig. 2). Consequently, the conversion factor for silicon is found at 427 counts/s/%. This value was successfully confirmed by a calibration test on quartz leading also to a value of 427 counts/s/%.

The H/S ratio is an important factor because it influences the molar mass of C–S–H and the mass concentration of silicon and calcium. If H/S = 1.2 as proposed by Ref. [19] for dried C–S–H, the conversion factor of silicon is estimated at 368 counts/s/%. In the case of H/S = 3.0 as mentioned in Ref. [20] for saturated C_3S pastes, this conversion factor becomes equal to 514 counts/s/%. The mass conversion factor determined from quartz standard (427 counts/s/%) is not found with the H/S values of 1.2 and 3.0. Consequently, the water content in C–S–H is reliably characterized by the molar H/S ratio of 2.1.

The calcium and silicon profiles were converted in mass content using the factors previously found on portlandite and C–S–H (Fig. 3). The molar C/S ratio was estimated at locations where C–S–H were identified on the microprobe profiles. On the basis of 18 points, the average molar C/S ratio was found at 1.67 ± 0.03 in accordance with Ref. [18]. It is also noticed that the mass concentration of calcium in locations where calcium and silicon profiles match is lower than 35% corresponding to C–S–H. There is no correlation between the calcium and silicon contents indicating the presence of C_3S for which the mass concentration of calcium is 53%. That confirms the previous observations showing that the pastes did not contain unhydrated C_3S and that they were only constituted by portlandite and C–S–H. Consequently, silicon was assumed to be only present in C–S–H.

3.2. CH content

The molar C/S ratio was previously found at 1.67. Consequently, the mass Ca/Si ratio in C–S–H was estimated at 2.30. For each microprobe profile, the mass concentration of calcium in C–S–H was determined as $Ca/Si \times Si^{\%mass}_{C-S-H}$. The calcium profile $Ca/Si \times Si^{\%mass}_{C-S-H}$ is plotted in Fig. 3(a). This profile is equivalent to the total calcium profile where C–S–H are identified. The mass concentration of calcium in portlandite $Ca^{\%mass}_{CH}$ is given by:

$$Ca^{\%mass}_{CH} = \underbrace{Ca^{\%mass}_{total}}_{Experimental} - \underbrace{Ca^{\%mass}_{C-S-H}}_{Si^{\%mass}_{C-S-H} \times Ca/Si} \quad (3)$$

Fig. 3(b) presents the profile of the calcium mass concentration in portlandite. The portlandite mass content η_{CH} can be expressed as follows :

$$\eta_{CH} = \frac{M_{CH}}{M_{Ca}} Ca^{\%mass}_{CH} \quad (4)$$

where M_{CH} is the molar mass of portlandite (74.09 g/mol).

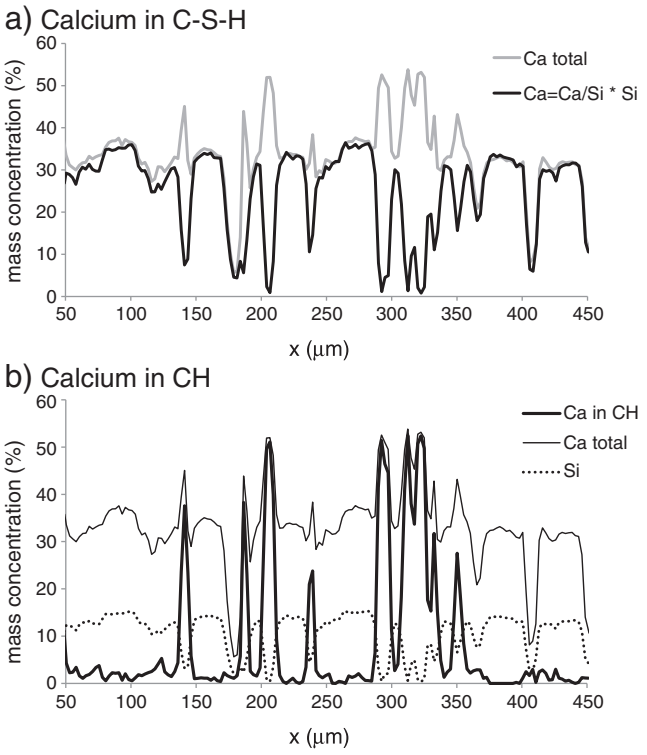

Fig. 3. Determination of calcium content in CH.

Eq. (4) gives the mass concentration of portlandite for each point of the microprobe profile. An average value of η_{CH} and its standard deviation were calculated throughout the thickness of the samples on the basis of 10 microprobe profiles using 500 points per profile. The portlandite mass content in hydrated C_3S paste was estimated at 24.4 ± 2.3%. Fig. 4 shows the cumulative function in accordance with a normal law.

In addition, a thermogravimetric analysis (TGA) was performed. TGA is commonly used to estimate the portlandite content in cementitious materials [3,12]. TGA analyses were carried out on very small pieces of hydrated C_3S pastes (~15 mg) with a PerkinElmer TGA 7. Fig. 5 shows the mass evolution and the differential thermal analysis as a function of temperature measured by TGA. The mass loss around 420 °C is attributed to the water loss due to the decomposition of portlandite. This mass loss was calculated from both curves according to the annotations in Fig. 5: (A) by mass loss between the points A_1 and B_1, (B) by integrating the derivative between the points A and B with a baseline at the level of the point B, and (C) by integrating the derivative between the points A and B with the baseline AB. The sample was partially saturated before the TGA test as evidenced by the mass loss between 30 °C and 100 °C in Fig. 5. The reference mass was taken at the temperature of 105 °C for which the evaporable

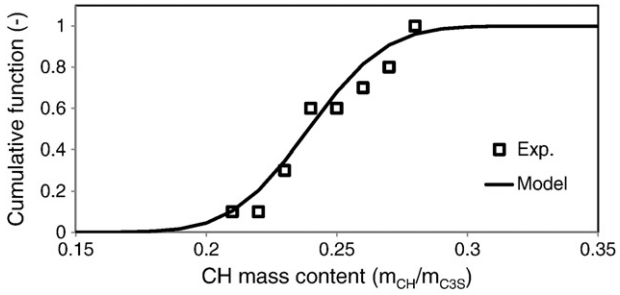

Fig. 4. Cumulative function of the CH contents calculated on the microprobe profiles according to a normal law.

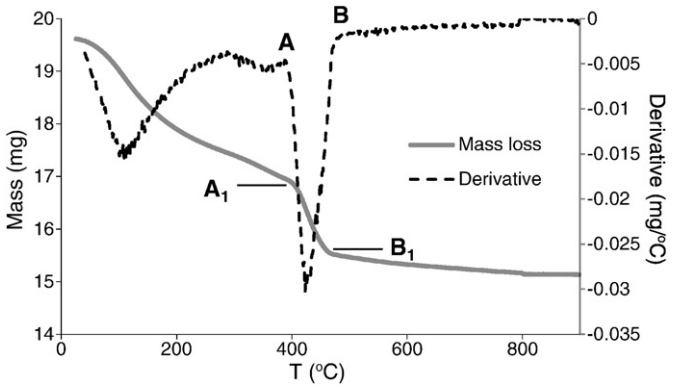

Fig. 5. TGA measurements for determining the $Ca(OH)_2$ content.

water is assumed to be lost. The calculations of the mass content of portlandite led to: (A) 29.7%, (B) 27.8%, and (C) 25.6%. For method (A), the mass loss was assumed to totally come from the decomposition of the portlandite only while evaporation of adsorbed water certainly occurred in parallel. The integration of the derivative allowed to distinguish the portlandite decomposition and the water evaporation by considering the baseline in the calculation of the area under the curve. For the case (B), the baseline was assumed to be at the level of the point B after which the derivative was almost constant while the line AB was considered as the baseline in the case (C). The point A probably should be influenced by a mass loss just before the portlandite decomposition, and the method (C) has overestimated the mass loss. The method (B) likely provided the more reliable CH mass content with a consistent estimation of the water evaporation simultaneous to the CH decomposition. This analysis globally gives a higher CH mass content compared to the microprobe method. The methods (A), (B), and (C) show the limits of TGA to give consistent results in this work. Moreover, the difficulty to control the initial mass of the sample due to the uncertainty of its degree of saturation leads to inaccurate mass content estimation. However, TGA analysis has confirmed the absence of carbonation; no mass loss was detected between 700 and 900 °C, which corresponds to the temperature range of calcium carbonate decomposition [3].

The portlandite mass content found from the microprobe analysis was consistent with previous works on tricalcium silicate, such as in Ref. [10] (25%), where a TGA technique on C_3S compacts was used. The authors in Ref. [9] used a water adsorption technique to obtain 24.7% after 28 days of hydration and 29.2% after 60 days. But in the latter hydration time, free lime was suspected to be present. Different works have given data slightly higher, between 30% and 35% by Quantitative X-Ray Analysis [11,13] and chemical method [21], while a portlandite mass content around 20% was also found [12] by differential thermal technique.

4. Diffusion tests

4.1. Experimental

Fig. 6 shows the diffusion set up used to determine the ionic diffusion coefficients of hydrated C_3S pastes. An adapted bearing was manufactured for the small C_3S disks (Fig. 6(a)). The C_3S samples were fixed between two cells with the bearing. The sample surface, exposed to the cell solutions, was 3.8 cm^2. The volume of the cells was 0.1 l. The upstream cell was filled with NaOH (0.32 M) and NaCl (two different test conditions at 0.1 and 0.05 M) solution while the downstream contained 0.32 M NaOH solution (Fig. 6(b)). The solutions were renewed on a weekly basis. Upon renewing solutions, chloride concentration in the downstream cell was measured to obtain the cumulative chloride flux across the sample. The chloride

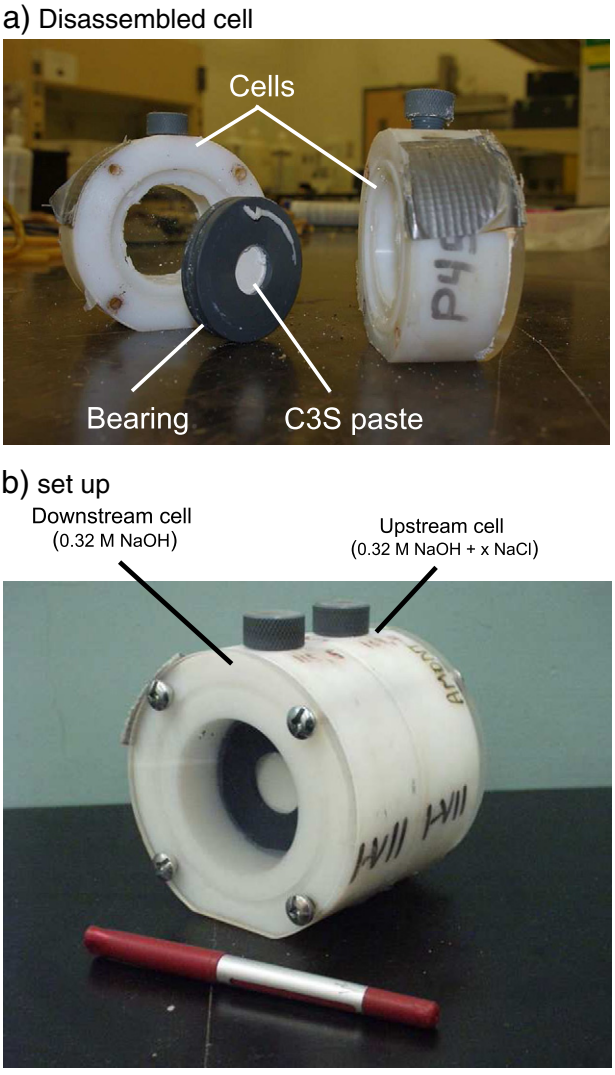

Fig. 6. Diffusion cell.

concentration was measured with a Mettler D21 titrator using a silver electrode Mettler Toledo DM 141-SC. Diffusion tests were performed over 50 days.

The chloride concentration evolution in the downstream cell was the sum of the successive measured concentrations. As shown in Fig. 7, the measured chloride concentration was linear as a function of time. There was no time lag corresponding to the necessary time for chloride ions to pass through the disk thickness. The very small thickness of the samples (1.5 mm) explained this absence of time lag. Consequently, the steady-state was rapidly reached as illustrated by the linear behavior. It could be noted that the chloride concentration in the downstream cell between two measurements remained too low to influence the diffusion kinetics; the boundary conditions were thus considered constant during the test. As expected, the chlorideingress was faster for 0.1 M than for 0.05 M.

4.2. Numerical model

The ionic transport model STADIUM® was used to analyze the diffusion test results [14,22]. It is based on a Sequential Non Iterative Algorithm (SNIA) that separately solves the transport equations and the chemical equilibrium relationships. The transport equations (i.e. mass conservation equations for the species, moisture flow, thermal conduction, and electrodiffusion coupling) are discretized using the finite element method and solved simultaneously using a coupled

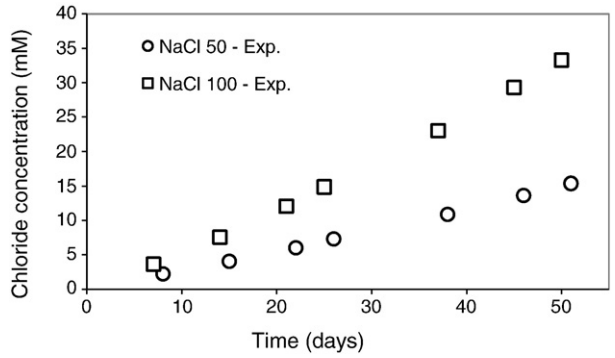

Fig. 7. Chloride concentration in the downstream cell during diffusion tests for NaCl = 0.05 M and 0.1 M in the upstream.

algorithm. From expressions at the microscopic scale, the mass conservation equations were integrated over a representative elementary volume (REV) using a homogenization technique, to yield expressions at the macroscopic scale [23,24]. In the case of saturated materials maintained under isothermal conditions, the advection effect on the ionic flux can be neglected and the mass conservation equation for species *i* is then expressed as [14]:

$$\frac{\partial(\phi c_i)}{\partial t} = -\frac{\partial J_i}{\partial x} = \frac{\partial}{\partial x}\left(\underbrace{\phi D_i \frac{\partial c_i}{\partial x}}_{\text{diffusion}} + \underbrace{\phi \frac{z_i F}{RT} D_i c_i \frac{\partial \Psi}{\partial x}}_{nsmallmatrix\text{electrical coupling}} + \underbrace{\phi D_i c_i \frac{\partial ln\gamma_i}{\partial x}}_{\text{chemical activity}} \right) \quad (5)$$

where J_i is the flux (mol/m^2/s), c_i is the concentration (mmol/l), D_i is the diffusion coefficient (m^2/s), z_i is the valence number of the ionic species *i*. ϕ is the porosity (m^3/m^3), F is the Faraday constant (96488.5 C/mol), Ψ is the electro-diffusion potential (V), R is the ideal gas constant (8.31 J/mol/K), T is the temperature (K), and γ_i is the activity coefficient. The activity coefficients in the model are evaluated on the basis of the Harvie, Moller and Weare (HMW) implementation of Pitzer's ion interaction model [25]. D_i is defined as

$$D_i = \tau D_i^0 \quad (6)$$

where D_i^0 is the self-diffusion coefficient of species *i* and τ is the tortuosity.

The ion *i* interacts with the other ions in the pore solution as a result of their electrical charges. This electrostatic interaction induces an electrical potential and influences their motion in the porous network of the material. As outlined in Eq. (5), the electrostatic effect on ionic species *i* is called *electrical coupling*. Poisson's equation (Eq. 7) is added to Nernst-Planck equation to solve the electro-diffusion potential variable. The averaged version of Poisson's equation is given by [14]:

$$\frac{d}{dx}\left(\tau\phi\frac{d\Psi}{dx}\right) = -\frac{F}{\varepsilon}\phi\sum_{i=1}^{N} z_i c_i \quad (7)$$

where ε is the medium permittivity (F/m), and N the number of ionic species in the pore solution. $\varepsilon = \varepsilon_r \varepsilon_0$ with ε_r, the vacuum permittivity ($8.854\,10^{-12}$ F/m) and ε_0, the dielectric constant of water (80 at 20 °C).

The presence of 0.32 M NaOH in the upstream and the downstream cells allowed maintaining the equilibrium between the hydrates and the exposure solutions. It was assumed that the properties of hydrated C_3S pastes remained unchanged since the portlandite and C–S–H are not affected in highly basic solutions. It was also assumed that there were no chemical reactions between chloride ions and the cementitious matrix during the diffusion experiments

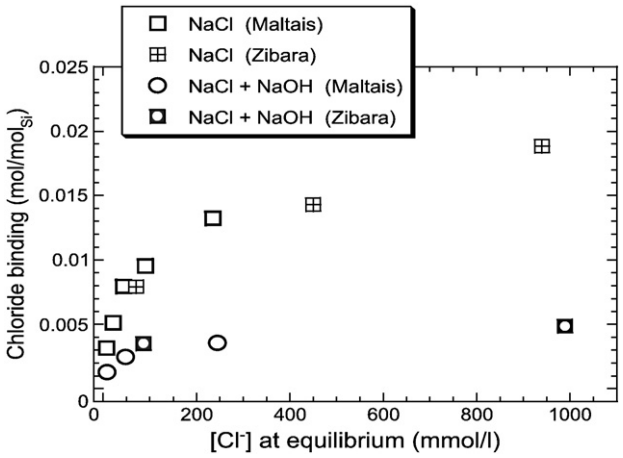

Fig. 8. effect of NaOH on the chloride binding in the case of hydrated C_3S pastes [26–29].

since aluminates were not present in the material. Furthermore, in the presence of high NaOH concentration, the physical adsorption of chloride on C–S–H surface is assumed to be very low in accordance with refs. [26,27] and [28] (Fig. 8). Calculations with STADIUM® confirmed that the motion of chloride ions was not influenced by physical interaction. The evolution of the chloride concentration in the downstream was characterized by the absence of time lag and by the linear behavior. These two points corroborates that physical binding of chloride ions and chemical reactions in the CH/C–S–H system were assumed to be negligible to consider a pure diffusion case with only a correction to account for electrostatic interactions between ions.

4.3. Modeling results

The ionic species Ca^{2+}, OH^-, Na^+, and Cl^- were taken into account in the calculations. The initial composition of the pore solution was $[OH^-]$=0.04 M and $[Ca^{2+}]$=0.02 M, corresponding to the equilibrium concentration of the CH/C–S–H system. As mentioned previously, the porosity of the hydrated C_3S was 35%. The diffusion coefficient D_i of the species *i* was determined by inverse analysis by using STADIUM® to replicate the experimental curves given in Fig. 7. The chloride concentration in the downstream cell is given by:

$$[Cl^-] = \frac{J_{Cl^-} \times S \times t}{V} \quad (8)$$

where J_{Cl^-} (mol/m^2/s) is the chloride ions flux at the sample surface S (m^2) exposed to the downstream cell (Eq. 5), t is the diffusion time (s), and V is the volume of the downstream cell (L). The surface S and the volume V are 3.8 cm^2 and 0.1 L respectively. The calculations performed with STADIUM® lead to a tortuosity $\tau = 3.89\ 10^{-2}$. This

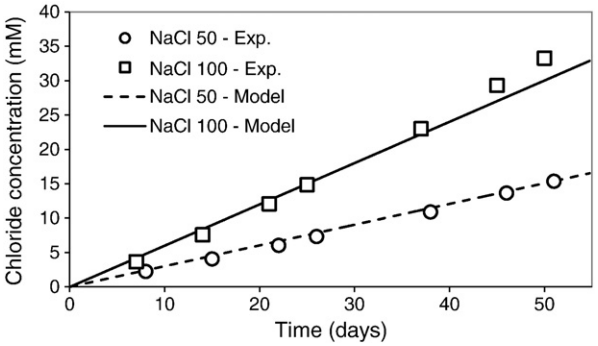

Fig. 9. Modeling of diffusion tests with $D_{Cl^-} = 7.9010{-}11 m^2/_s$.

Table 1
Diffusion coefficient of the different species for the hydrated C_3S pastes.

Species	Diffusion coefficient D_i (10^{-11} m^2/s)
OH^-	20.50
Cl^-	7.90
Na^+	5.24
Ca^{2+}	3.08

tortuosity value is equivalent to $D_{Cl^-} = 7.90\ 10^{-11}\ m^2/s$ (Eq. 6). Fig. 9 shows the results of the simulations with this value of D_{Cl^-}. Table 1 gives the diffusion coefficient of the various species present in the studied system.

5. Conclusion

This paper presented a reliable method based on electron microprobe measurements to determine the portlandite content and the molar ratio C/S of C–S–H of hydrated C_3S pastes. The portlandite mass content was found at 24.4% ± 2.3%. The microprobe analysis provided an averaged value through the thickness of the samples. Additionally, the diffusion coefficient of ions was determined from analyzing diffusion test results with the numerical model STADIUM®. The results provided essential parameters to model the behavior of these C_3S-based materials in the presence of aggressive solutions. Based on this work, the leaching of portlandite and the decalcification of C–S–H could be investigated of hydrated C_3S paste samples exposed to low pH environment.

Acknowledgements

The authors are grateful to J.J. Beaudoin from the National Research Council (Canada) for providing the C_3S samples.

References

[1] A. Delagrave, B. Gérard, J. Marchand, Modeling the calcium leaching mechanisms in hydrated cement pastes, in: K.L. Scrivener, J.F. Young (Eds.), Mechanisms of Chemical Degradation of Cement-based Systems, E & FN SPON, 1997.
[2] K. Haga, S. Sutou, M. Hironaga, S. Tanaka, S. Nagasaki, Effects of porosity on leaching of Ca from hardened ordinary portland cement paste, Cem. Concr. Res. 35 (2005) 1764–1775.
[3] H.F.W. Taylor, Cement Chemistry, 2nd Edition Academic Press, London, 1997.
[4] J.F. Young, H.S. Tong, R.L. Berger, Compositions of solutions in contact with hydrating tricalcium silicate pastes, J. Am. Ceram. Soc. 60 (5–6) (1977) 193–198.
[5] L.S.D. Glasser, E.E. Lachowski, K. Mohan, H.F.W. Taylor, A multi-method study of C-3S hydration, Cem. Concr. Res. 8 (1978) 733–740.
[6] D.L. Kantro, S. Brunauer, C.H. Weise, Development of surface in the hydration of calcium silicates. II. extension of investigations to earlier and later stages of hydration, J. Phys. Chem. 66 (1962) 1804–1809.
[7] H.F.W. Taylor, D.E. Newbury, Calcium hydroxide distribution and calcium silicate hydrate composition in tricalcium silicate and β-dicalcium silicate, Cem. Concr. Res. 14 (1984) 93–98.
[8] I.G. Richardson, The calcium silicate hydrates, Cem. Concr. Res. 38 (2008) 137–158.
[9] R.A. Olson, H.M. Jennings, Estimation of C-S-H content in a blended cement paste using water adsorption, Cem. Concr. Res. 31 (2001) 351–356.
[10] S. Catinaud, J.J. Beaudoin, J. Marchand, Influence of limestone addition on calcium leaching mechanisms in cement-based materials, Cem. Concr. Res. 30 (2000) 1961–1968.
[11] S. Brunauer, D.K. Kantro, L.E. Copeland, The stoichiometry of the hydration of β-dicalcium silicate and tricalcium silicate at room temperature, J. Am. Chem. Soc. 80 (4) (1958) 761–767.
[12] V.S. Ramachadran, Differential thermal method of estimating calcium hydroxide in calcium silicate and cement pastes, Cem. Concr. Res. 9 (1979) 677–684.
[13] I. Odler, J. Schuppstuhl, Combined hydration of tricalcium silicate and β-dicalcium silicate, Cem. Concr. Res. 12 (1982) 13–20.
[14] E. Samson, J. Marchand, Modeling the transport of ions in unsaturated cement-based materials, Comput. Struct. 85 (2007) 1740–1756.
[15] J.J. Beaudoin, S. Catinaud, J. Marchand, S. T, Volume stability of hydrated portland cement phases exposed to aggressive solutions, Indust. It. Cemento 782 (2002) 954–967.
[16] V.S. Ramachandran, Concrete Admixtures Handbook: Properties, Science, and Technology, 2nd Edition Noyes Publications, New-York, 1995.
[17] G.A. Desborough, R.H. Heidel, G.K. Czamanske, Improved quantitative electron microprobe analysis at low operating voltage: Ii. sulfur, Am. Mineral. 56 (1971) 2136–2141.
[18] B. Lothenbach, T. Matschei, G. Möschner, F.P. Glasser, Thermodynamic modeling of the effect of temperature on the hydration and porosity of portland cement, Cem. Concr. Res. 38 (2008) 1–18.
[19] J.J. Thomas, H.M. Jennings, A.J. Allen, Relationships between composition and density of tobermorite, jennite, and nanoscale cao-sio$_2$-h$_2$o, J. Phys. Chem. C 114 (2010) 7594–7601.
[20] H.J.H. Brouwers, The work of Powers and Brownyard revisited: part i, Cem. Concr. Res. 34 (2004) 1697–1716.
[21] E.E. Pressler, S. Brunauer, D.L. Kantro, C.H. Weise, Determination of the free calcium hydroxide contents of hydrated portland cements and calcium silicates, Anal. Chem. 33 (7) (1961) 877–882.
[22] E. Samson, J. Marchand, K. Snyder, Calculations of ionic diffusion coefficients on the basis of migration test results, Mater. Struct. 36 (2003) 156–165.
[23] J. Bear, Y. Bachmat, Introduction to Modeling of Transport Phenomena in Porous Media, Kluwer Academic Publishers, Netherlands, 1991.
[24] E. Samson, J. Marchand, J.J. Beaudoin, Describing ion diffusion mechanisms in cement-based materials using the homogenization technique, Cem. Concr. Res. 29 (8) (1999) 1341–1345.
[25] G. Zhang, Z. Zheng, J. Wan, Modeling reactive geochemical transport of concentrated aqueous solutions, Water Resour. Res. 41 (2005) W02018, doi: 10.1029/2004WR003097.
[26] H. Zibara, Binding of external chlorides by cement pastes, Ph.D. thesis, University of Toronto (2001).
[27] Y. Maltais, J. Marchand, P. Henocq, T. Zhang, J. Duchesne, Ionic interactions in cement-based materials: Importance of physical and chemical interactions in presence of chloride or sulfate ions, in: J. Skalny (Ed.), Materials Science of Concrete VII, The American Ceramic Society, 2004.
[28] P. Henocq, Modélisation des interactions ioniques à la surface des silicates de calcium hydratés, Ph.D. thesis, Laval University, Canada (2005).
[29] Y. Maltais, Contribution à l'étude des mécanismes de transport ionique et de dégradation chimique dans les matériaux cimentaires partiellement ou complètement saturés, Ph.D. thesis, Laval University, Canada (2005).